2016

Observation of diurnal variations in mesoscale eddy sea-surface currents using GOCI data

Ji-Eun Park

Kyung-Ae Park

See next page for additional authors

Citation/Publisher Attribution

Ji-Eun Park, Kyung-Ae Park, David S. Ullman, Peter C. Cornillon & Young-Je Park (2016) Observation of diurnal variations in mesoscale eddy sea-surface currents using GOCI data, Remote Sensing Letters, 7:12, 1131-1140, DOI: 10.1080/2150704X.2016.12194
Available at: https://doi.org/10.1080/2150704X.2016.1219423

Taylor & Francis
Taylor & Francis Group

Remote Sensing Letters

ISSN: 2150-704X (Print) 2150-7058 (Online) Journal homepage: https://www.tandfonline.com/loi/trsl20

Observation of diurnal variations in mesoscale eddy sea-surface currents using GOCI data

Ji-Eun Park, Kyung-Ae Park, David S. Ullman, Peter C. Cornillon & Young-Je Park

To cite this article: Ji-Eun Park, Kyung-Ae Park, David S. Ullman, Peter C. Cornillon & Young-Je Park (2016) Observation of diurnal variations in mesoscale eddy sea-surface currents using GOCI data, Remote Sensing Letters, 7:12, 1131-1140, DOI: 10.1080/2150704X.2016.1219423

To link to this article: https://doi.org/10.1080/2150704X.2016.1219423

Published online: 19 Aug 2016.

REMOTE SENSING LETTERS, 2016
VOL. 7, NO. 12, 1131–1140
http://dx.doi.org/10.1080/2150704X.2016.1219423

Taylor & Francis
Taylor & Francis Group

OPEN ACCESS

Observation of diurnal variations in mesoscale eddy sea-surface currents using GOCI data

Ji-Eun Park [a], Kyung-Ae Park[b], David S. Ullman[c], Peter C. Cornillon[c] and Young-Je Park[d]

[a]Department of Science Education, Seoul National University, Seoul, South Korea; [b]Department of Earth Science Education, Research Institute of Oceanography, Center for Education Research, Seoul National University, Seoul, South Korea; [c]Graduate School of Oceanography, University of Rhode Island, Kingston, Rhode Island, USA; [d]Korea Ocean Satellite Center, Korea Institute of Ocean Science & Technology, Ansan, South Korea

ABSTRACT

The surface current field of a mesoscale eddy in the East Sea (Sea of Japan) was derived from consecutive Geostationary Ocean Color Imager chlorophyll-*a* (chl-*a*) concentration images using the normalized maximum cross-correlation method. The estimated current field of the eddy exhibited anticyclonic structure demonstrated by the objective dynamic thresholds of correlation coefficients. The eddy periphery was defined by fitting an ellipse to subjectively selected points from the frontal map of chl-*a* concentration data. Radial distribution and hourly variation of the current speed around the eddy were presented. In terms of the magnitude and direction, the estimated current field was in good agreement with altimeter-based current field and current vectors from surface drifters. Diurnal variations in the current speeds of the mesoscale eddies showed a quadratic relation to the wind speed.

ARTICLE HISTORY
Received 24 March 2016
Accepted 22 July 2016

1. Introduction

The East Sea (Sea of Japan) (EJS) is one of semi-enclosed seas connected to the Pacific Ocean by relatively low and narrow straits (Figure 1(*a*)). Sea surface temperature (SST) measurements from the National Oceanic and Atmospheric Administration-19's Advanced Very High Resolution Radiometer on 5 April 2011 (Figure 1(*b*)) indicated turbulent and coherent spatial structures such as filaments, plumes and mushroom-like features as well as mesoscale eddies in the EJS (Isoda and Saitoh 1993; Isoda 1994; Morimoto, Yanagi, and Kaneko 2000). These mesoscale eddies were formed near the subpolar frontal zone in the EJS (e.g., Park et al. 2007) and can play significant roles in transferring kinetic energy and mixing substances in the upper ocean, affecting marine ecosystems through supplying nutrients that feed the base of the food chain from the subsurface (Yoder et al. 1983).

Many well-known pioneering studies have utilized various kinds of satellite data and satellite-tracked surface drifter data to investigate the physical and biological characteristics of eddies and their horizontal structures (Hooker and Brown 1994). Analyses of satellite SST images and scatterometer wind field data illustrated that the spatial structure

CONTACT Kyung-Ae Park kapark@snu.ac.kr Department of Earth Science Education, Research Institute of Oceanography, Center for Education Research, Seoul National University, Seoul, Korea

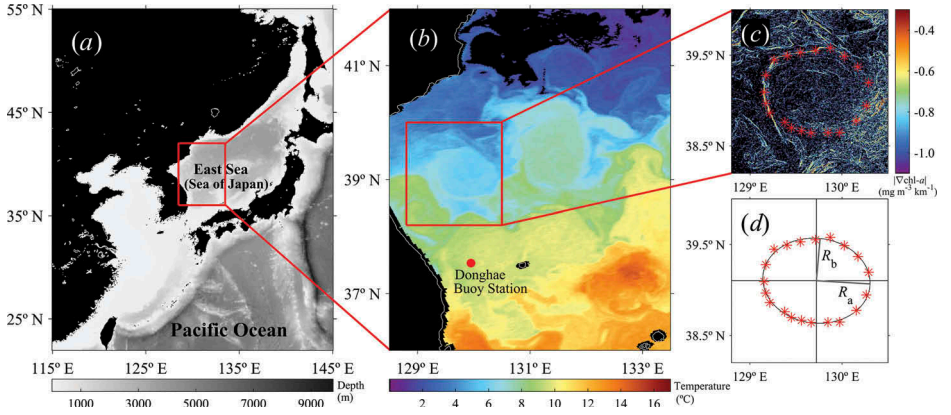

Figure 1. (*a*) Bathymetry in the study area (a red box) of the East Sea (Sea of Japan). (*b*) A sea surface temperature image from NOAA-19/AVHRR showing mesoscale eddy structures on 5 April 2011, where the red dot denotes the Donghae buoy station. (*c*) Distribution of fronts from a GOCI chlorophyll-*a* concentration image, where the red stars represent the subjectively digitized points along the periphery of the eddy. (*d*) A least-square fitted ellipse using geolocation information of (*c*), where R_a and R_b are the semi major and semi minor axis lengths, respectively.

of a Gulf-Stream ring through eddy-induced stability change in the marine-atmospheric boundary layer (Chelton et al. 2004; Park, Cornillon, and Codiga 2006). Oceanic eddies in the EJS have been also studied through satellite data such as infrared images and sea surface height (SSH) anomalies (Isoda and Saitoh 1993; Morimoto, Yanagi, and Kaneko 2000). Recently, Park, Woo and Ryu (2012) estimated the sizes of the eddies from Geostationary Ocean Color Imager (GOCI) chlorophyll-*a* (chl-*a*) concentration images and addressed their dependence on meridional changes of Rossby deformation radius.

Since the first application of maximum cross-correlation (MCC) method to the atmospheric cloud movement (Leese, Novak, and Clarke 1971), this method has been used to estimate advective sea-surface current vectors from consecutive infrared or SST images (e.g., Emery et al. 1986). Very recently, not only the SST images but also ocean colour images, like chl-*a* images or suspended sediment concentration images, have been used as a method of tracking sea-surface movement (Yang et al. 2014).

However, none of the previous studies has revealed the radial structure of these eddies or their short-term variations for a day so far. Thus, this study aims to derive surface current field around mesoscale eddy from consecutive images of GOCI and validate this estimation using the geostrophic current field derived from satellite altimeter data to estimate the radial velocity structure of mesoscale eddy, to validate the estimated current field to geostrophic current field from satellite altimeter data and to investigate diurnal variation of the current field.

2. Data and methods

2.1. *Satellite data and wind data*

After extensive review of GOCI level-1 data (~500 m × 500 m), images from 31 March 2011 and 5 April 2011 were chosen in order to obtain chl-*a* images without cloud (clear

sky). The Ocean Color 2 chl-*a* algorithm of the National Aeronautics and Space Administration/Goddard Space Flight Center and standard atmospheric correction of GOCI data were applied during the conversion process (Ahn et al. 2012). To validate the estimated currents, we used satellite-tracked surface drifter data from the Atlantic Oceanographic and Meteorological Laboratory and altimeter-based Maps of Absolute Dynamic Topography (0.25° × 0.25°) provided by the Archiving, Validation and Interpretation of Satellite Oceanographic. To investigate the current and wind forcing, we used hourly wind measurements at Donghae buoy station (129.9°E, 37.5°N), as shown in Figure 1(*b*), and 6-h ERA-interim wind data from the European Centre for Medium-Range Weather Forecasts (ECMWF).

2.2. *Ellipse fitting along eddy periphery*

To identify an eddy and calculate the radial distance of each point from the eddy centre, we extracted geolocation information for the eddy boundary from the frontal map of a GOCI chl-*a* image. The frontal value was calculated from the magnitude of the 2D gradient of chl-*a* ($|\nabla \text{chl}{-}a|$) (Figure 1(*c*)). After subjectively selecting points with large frontal values along the periphery of the eddy (marked in red stars in Figure 1(*c*)), we applied an ellipse equation with a tilting angle to determine the centre (latitude and longitude), tilting angle, major and minor axis lengths (R_a and R_b, respectively) and eccentricity of an eddy, as shown in Figure 1(*d*) (Park, Cornillon, and Codiga 2006).

2.3. *Estimation of current vectors*

The normalized maximum cross-correlation (NMCC) method was utilized to derive the surface current field from the time-consecutive satellite images. The NMCC method uses template matching for feature tracking, finding the location that has the MCC between two normalized images (Lewis 1995). Using the two time-successive GOCI chl-*a* images, the normalized cross-correlation coefficients (ρ) were calculated within a search tile (43 × 43 pixels) between two submatrices of each image with a size of 23 × 23 pixels according to a sensitivity test using various window sizes. The size of the search window was determined by considering the maximum current speed measured by the HF radar, surface drifters and altimeters in this region. Considering the spatial resolution of GOCI and the potential magnitude of the current field in the study region, in order to represent the movement of oceanic surface features properly, we determined that 2 h was the minimum temporal interval instead of GOCI's observation interval of an hour.

2.4. *Dynamic threshold of correlation coefficient*

After considering the available degrees of freedom in determining the surface current field, a window-dependent varying threshold (hereafter dynamic threshold) of a template window (23 × 23 pixels) was used for the calculation of ρ between two satellite images. The total number of pixels in the two images was divided by a square of autocorrelation length scale for each sub-image to calculate how many pixels of the sub-image pixels are independent (Emery et al. 1986; Ninnis, Emery, and Collins 1986). After finding the degree of freedom, the rejection region using ρ as a critical threshold at

each pixel was objectively determined by Pearson's correlation coefficient table with 95% significance level. Emery et al. (1986) assumed the same autocorrelation length scale in one image; however, this study adopted a dynamic threshold that adapted to the oceanic features within the window in the image. Statistically-insignificant vectors with high *p*-values (>0.05) were eliminated.

3. Results

3.1. *Eddy current field using dynamic thresholds*

Figure 2 shows an example of the current derivation of the two mesoscale eddies using GOCI chl-*a* images at 10:30 and 12:30 (local time) on 31 March 2011. Relatively high cut-off thresholds ($\rho > 0.7$) were found along the periphery and outside of the eddy, which was in contrast to the inside of the eddy with relatively low values ($\rho < 0.5$) (Figure 2(*a*)). After consideration of the spatial scales and degree of freedom and distribution of the dynamic thresholds, ρ value at each pixel exhibited a distinct spatial structure as shown in Figure 2(*b*). Inside of the eddy, the critical values were almost uniform at about 0.2 or less. Applying this, dynamic threshold produced different surface current vectors in the eddy interior compared to the case of applying a fixed cut-off coefficient of 0.4 suggested by Emery et al. (1986) (Figure 2(*c*)). This was further supported by the estimated current vectors and is shown in Figure 2(*f*). This analysis clearly revealed the spatially complicated structure, even inside the eddy, through the use of a dynamic threshold (Figure 2(*e*)). In addition to anticlockwise rotary motions inside the eddy, the spatial structure of the swirling current was presented in detail with high velocity (~0.6 m s^{-1}) near the eddy boundary whilst being much lower about 0.2 m s^{-1} for a radial distance ratio (r/R) of less than 0.3 in the eddy interior (Figure 2(*f*)), where r is the distance of each position from the centre and R is the directional radius of the ellipse considering its tilting angle.

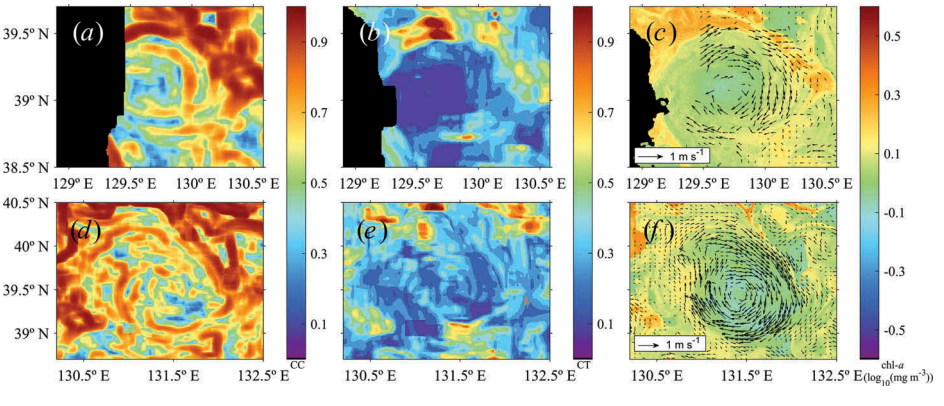

Figure 2. (*a*) An example of correlation coefficients (CC) between two consecutive chlorophyll-*a* concentration images (10:30 and 12:30 local time) around an eddy on 31 March 2011. (*b*) Spatial distribution of dynamic correlation coefficients as a critical threshold (CT), corresponding to each pixel. (*c*) The current vectors re-estimated by applying the different dynamic threshold every pixel. (*d*)–(*f*) The results of the estimated current vectors around another eddy on the same date.

3.2. *Spatial distribution of eddy current*

To analyse the spatial structure of eddy currents, we selected four eddies that appeared in GOCI chl-*a* images on 5 April 2011. These were given the names like Eddy 1, 2, 3 and 4 (hereafter E1, E2, E3 and E4) (Figure 3(*a*)). Eddy-induced chl-*a* distributions are not always consistent with the structure of eddies because of multiple regulating mechanisms (Siegel et al. 2011; Gaube et al. 2014). However, the closed contours of the SSH shown in Figure 3(*b*) confirmed the existence of each eddy, even for E3 with a relatively weak eastern boundary with E4. In spite of the small size of the EJS, the eddies revealed quite different spatial distribution of chl-*a*. Low chl-*a* values (<1.3 mg m^{-3}) appeared inside of E2 and E4 compared to the high values (~2.0 mg m^{-3}) near their peripheries. In contrast, these high chl-*a* appeared inside E1 and E3. These features are likely associated with different development stages of eddies or different biological responses to potential mechanisms such as eddy pumping, eddy advection and eddy-Ekman pumping processes as described by Siegel et al. (2011) and Gaube et al. (2014).

Figure 3(*c*) illustrated the distribution of ρ values around the eddies with greater values along the periphery of the eddy than inside. Figure 3(*d*) shows the distribution of dynamic ρ as a critical threshold obtained from degree of freedom calculations at each point. Similar to the distribution of ρ values, it was much larger along the eddy edge than inside. In this case, we filtered out vectors with statistically insignificant p values of greater than 0.05. The existence of the anticyclonic four eddies was clearly revealed through the application of dynamic thresholds as shown in the estimated current vectors (Figure 3(*e*)).

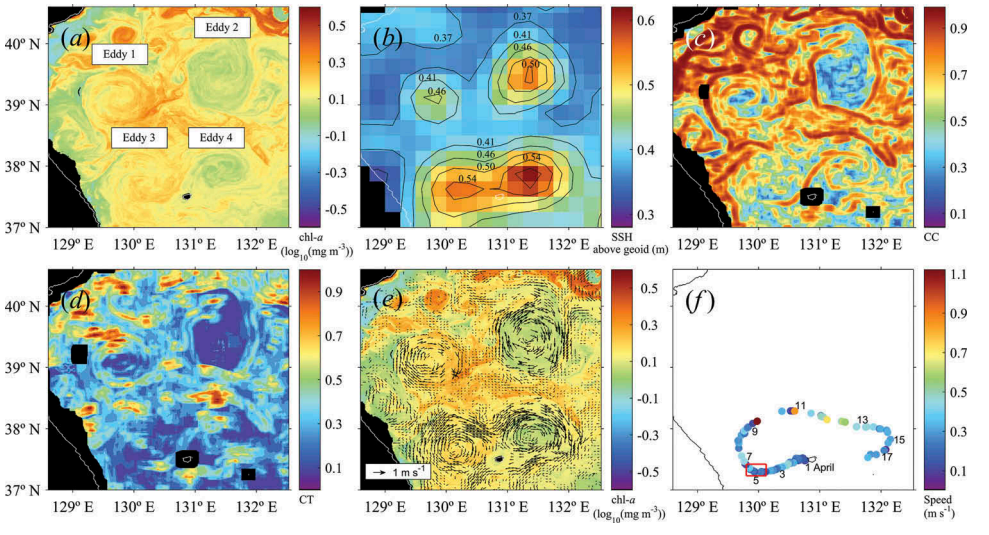

Figure 3. Spatial distribution of (*a*) GOCI chlorophyll-*a* concentration, (*b*) AVISO MADT height field, (*c*) correlation coefficients for the estimation of surface currents and (*d*) critical thresholds around the four eddies (Eddy 1–Eddy 4) on 5 April 2011. (*e*) Daily-averaged (9:30–16:30) surface current vectors derived from the NMCC method. (*f*) Track of a surface drifter on 1–17 April 2011 around Eddy 3 and Eddy 4 where the colours represent the estimated current speeds from the drifter and the red box denotes the drifter positions for the validation of (*e*).

3.3. *Validation with eddy current from ARGOS drifter and altimeter*

The estimated current speeds were validated with those from the ARGOS drifter, as indicated by the red box in Figure 3(*f*) and altimeter data in Figure 3(*b*). As a result, the estimated current speeds showed good agreement with the observed values based on root mean square (bias) errors of 0.065 m s^{-1} (0.021 m s^{-1}) and 0.15 m s^{-1} (0.089 m s^{-1}), respectively.

Synoptic *in-situ* measurements covering the four eddies were not readily available, so the estimated current vectors were validated through a comparison of the geostrophic current field calculated from the altimeter data with the daily-averaged current field derived from the NMCC (Figure 4). The altimeter-based current fields showed dominant anticyclonic motions around the eddies with low speeds (<0.05 m s^{-1}) near the centre and high speeds (~0.5 m s^{-1}) close to the inside boundary of the eddy (white lines in Figure 4(*a*)). E3 and E4 seemed to be in an initial stage for coalescence but still existed as isolated eddies with a dominant minimum of SSH at each centre. The current vectors of the two eddies near their boundary clearly showed opposite rotational directions: southward for E3 and northward E4 (box of Figure 4(*a*)).

The directions of our estimated current fields inside the four eddies are in agreement with those of the altimeter current field (Figure 4(*b*)). Zonal and meridional components of the estimated current vectors also demonstrated consistent results with the altimeter-derived current components (Figure 4(*c–d*)). Differences of greater than 0.1 m s^{-1} were found, implying overestimation of the values in the current field using the NMCC method. However, the altimeter data were objectively interpolated with a temporal correlation scale relatively longer than a day, possibly underestimating the instantaneous current speed.

3.4. *Radial distribution and hourly variation of eddy current speed*

Daily-averaged current speeds for four eddies were estimated as a function of distance from the eddy centre to investigate radial distribution of the current speed (Figure 5(*a*)). E2 had the largest mean radius ($\sqrt{\left(R_a^2 + R_b^2/2\right)}$ in Figure 1(*d*)) of 75 km among the eddies. Regarding the maximum of the binned averaged speeds within each eddy, E4 (51 km) was the fastest at 0.44 m s^{-1} and E1 (59 km) was the slowest at 0.29 m s^{-1}. The

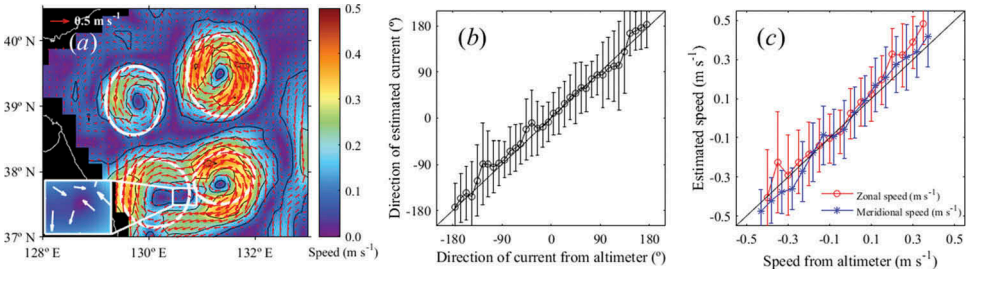

Figure 4. (*a*) Spatial distribution of surface current speed and current vectors estimated from satellite altimeter sea surface height data. Comparisons of the estimated current and altimeter-derived current in term of (*b*) direction, (c) zonal component (red) and meridional component (blue).

radial distribution of speeds showed a bell-shaped structure with relatively low speeds near the centre, the maximum occurring inside the eddy and a decrease approaching the outside of the eddy. As the velocity distribution depends on the radial position within the eddy, in order to understand where velocity reaches a maximum, we used the radial distance ratio (r/R) of each position. Figure 4(*b*) demonstrates that the maximum speed appears at the ratio (r/R) of 0.75 on average.

To examine the hourly variations in the current field of each eddy over a day, we estimated the current speeds over the 8-h period, 9:30–16:30 (Figure 5(*c–f*)). Overall, speeds for the four eddies ranged from a small speed of less than 0.01 m s^{-1} near the eddy centre to 0.4 m s^{-1} at the half of each eddy ($0.5 < r/R < 1$). Although these estimated speeds are relatively low in comparison with energetic Gulf-Stream rings with current speeds exceeding 1 m s^{-1} (Joyce and McDougall 1992), there were structural similarities to the Gulf-Stream warm rings in the distribution of speeds within the EJS eddies (e.g., Cornillon and Park 2001). On the whole, the speeds of all eddies (E1–E4) in the EJS demonstrated a bell-type pattern with respect to a radial distance.

3.5. *Role of wind forcing on diurnal variation of eddy current*

Such a diurnal variation of the eddy current except for tidal currents has been first reported in this study and its mechanism has not been clarified yet. The speed curves indicate relatively higher values at daytime, particularly at 14:30–16:30 in all eddies except E2. Surface warming over an eddy increases the wind speed through the air–sea stability change and feedback mechanisms (Park, Cornillon, and Codiga 2006). Our primary hypothesis is that short-term variations in the wind field, as a forcing that

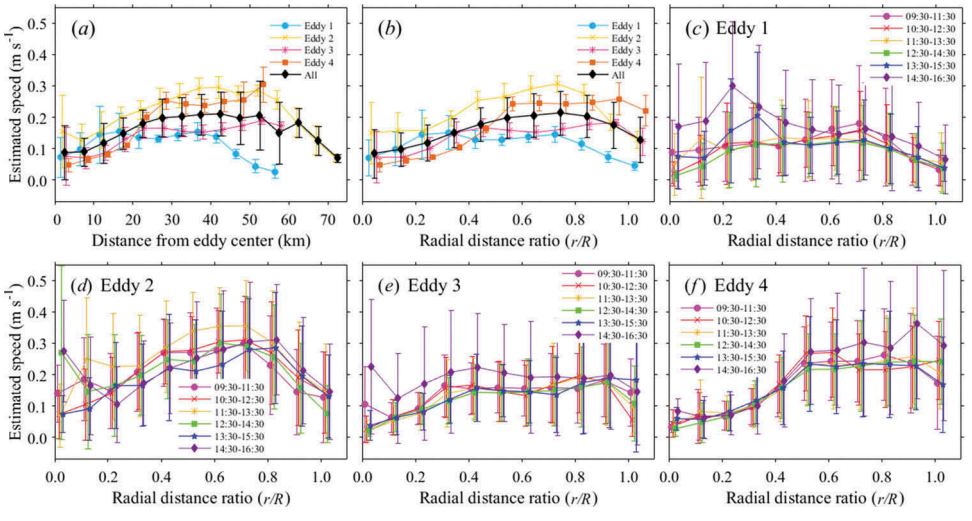

Figure 5. Radial distribution of the estimated current speeds as a function of (*a*) the distance (r) from the centre of eddies 1–4 and (*b*) the ratio (r/R) of this distance to the radial radius (R) of each eddy ellipse, where the error bar shows the mean error of each bin and the black line represents mean speeds averaged for all eddies. Hourly variations of estimated current speeds around each eddy as a function of the radial distance of (*c*) Eddy 1, (*d*) Eddy 2, (*e*) Eddy 3 and (*f*) Eddy 4 from 9:30 to 16:30 for a day.

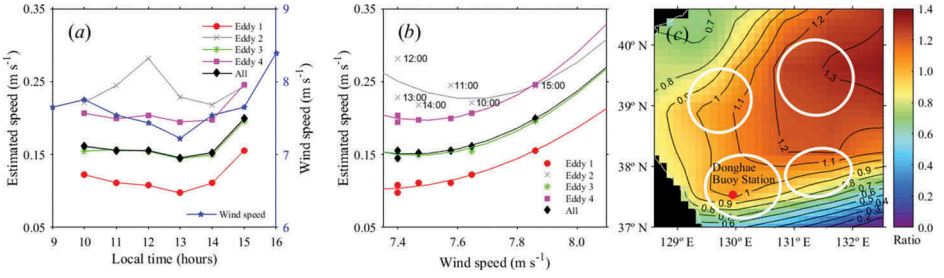

Figure 6. (*a*) Hourly variations of estimated current speeds of mesoscale eddies (Eddy 1–Eddy 4), where the blue line is wind speed measured at the Donghae buoy station. (*b*) Estimated current speeds as a function of wind speed, where the curved lines are quadratic least-square fits. (*c*) Ratio of ECMWF wind speed to ECMWF wind speed at the buoy station at 9:00 on 4 April 2011.

changes the velocity, would be responsible for the diurnal variation in the surface currents. Estimated speeds would have a quadratic relation with the wind speed. To test this, we investigated the relationship between the surface currents and hourly varying winds measured at the Donghae buoy station shown in Figure 1(*b*). The wind speeds varied from 7.2 m s^{-1} at 13:00 to 8.4 m s^{-1} at 16:00 (the blue line in Figure 6(*a*)). Note that the time-varying current speeds of the eddies (E1, E3 and E4) and their mean values (black line), in particular, presented a quite similar temporal pattern to the wind variations (blue line): a weak decrease up to 13:00 and strong increase at 15:00. In addition, the mean current speed ($\bar{U}$) for the mesoscale eddies (E1, E3 and E4) clearly showed a quadratic relation to the wind speed (W) ($\bar{U} = 0.27W^2 - 4.08W + 15.33$), as indicated by the fitted lines in Figure 6(*b*).

The ratio of ECMWF winds (Figure 6(*c*)) to the buoy wind near E3 at 9:00 was quite similar to that inside E1 (0.99) or E4 (0.96). In contrast, E2 (1.24) was exposed to much higher winds for an increase of 24% compared to E3. This implies that the buoy winds at E3 could not be applied to E2 with high hourly variations, as marked in grey in Figure 6 (*b*), because of the high spatial inhomogeneity of the wind field. Thus, it is highly plausible that the diurnal variation of the current speeds can be attributed to the short-term variations in the wind-forcing field. Therefore, we expect that the wind field has a crucial role in the diurnal variation of current speeds for mesoscale eddies in the EJS.

4. Summary and conclusion

Surface current vectors around an eddy were derived from GOCI chl-*a* data using the NMCC method. The fundamental assumption that chl-*a* is a conservative parameter seemed to be valid within the short-time periods of less than a few hours used in this study. We applied a dynamic threshold to determine an objective cut-off threshold by considering the degree of freedom and a decorrelation spatial scale. Using this method, the anticyclonic current field inside of the eddy was well represented, and daily-averaged currents from the NMCC method were well matched with altimeter-based geostrophic current in terms of the magnitude and direction. The radial structure of the estimated surface current speeds showed a bell-shaped structure with a maximum

speed at a distance ratio of around 0.75. For the first time using high-resolution GOCI optical data, this study presented the short-term (hourly) variations of the current field of mesoscale eddies in the EJS and the role of wind forcing on its diurnal variation contributing to the understanding of physio and biogeochemical processes of mesoscale eddies as one of elements of marine ecosystem.

Disclosure statement

No potential conflict of interest was reported by the authors.

Funding

This research was supported by the projects titled 'Research for Applications of Geostationary Ocean Color Imager (GOCI)' and 'Long-term change of structure and function in marine ecosystems of Korea' funded by the Ministry of Oceans and Fisheries, Korea.

ORCID

Ji-Eun Park http://orcid.org/0000-0002-5890-8877

References

Ahn, J.-H., Y.-J. Park, J.-H. Ryu, B. Lee, and I. S. Oh. 2012. "Development of Atmospheric Correction Algorithm for Geostationary Ocean Color Imager (GOCI)." *Ocean Science Journal* 47 (3): 247–259. doi:10.1007/s12601-012-0026-2.

Chelton, D. B., M. G. Schlax, M. H. Freilich, and R. F. Milliff. 2004. "Satellite Measurements Reveal Persistent Small-Scale Features in Ocean Winds." *Science* 303: 978–983. doi:10.1126/science.1091901.

Cornillon, P., and K.-A. Park. 2001. "Warm Core Ring Velocities Inferred from NSCAT Data." *Geophysical Research Letters* 28: 575–578. doi:10.1029/2000GL011487.

Emery, W. J., A. C. Thomas, M. J. Collins, W. R. Crawford, and D. L. Mackas. 1986. "An Objective Method for Computing Advective Surface Velocities from Sequential Infrared Satellite Images." *Journal of Geophysical Research* 91: 12865–12878. doi:10.1029/JC091iC11p12865.

Gaube, P., D. J. McGillicuddy, D. B. Chelton, M. J. Behrenfeld, and P. G. Strutton. 2014. "Regional Variations in the Influence of Mesoscale Eddies on Near-Surface Chlorophyll." *Journal of Geophysical Research: Oceans* 119: 8195–8220. doi:10.1002/2014jc010111.

Hooker, S. B., and J. W. Brown. 1994. "Warm Core Ring Dynamics Derived from Satellite Imagery." *Journal of Geophysical Research* 99: 25181–25194. doi:10.1029/94JC02171.

Isoda, Y. 1994. "Warm Eddy Movements in the Eastern Japan Sea." *Journal of Oceanography* 50: 1–15.

Isoda, Y., and S.-I. Saitoh. 1993. "The Northward Intruding Eddy along the East Coast of Korea." *Journal of Oceanography* 49: 443–458. doi:10.1007/BF02234959.

Joyce, T. M., and T. J. McDougall. 1992. "Physical Structure and Temporal Evolution of Gulf Stream Warm-Core Ring 82B." *Deep Sea Research Part A. Oceanographic Research Papers* 39 (1): S19–S44. doi:10.1016/S0198-0149(11)80003-8.

Leese, J. A., C. S. Novak, and B. B. Clarke. 1971. "An Automated Technique for Obtaining Cloud Motion from Geosynchronous Satellite Data Using Cross Correlation." *Journal of Applied Meteorology* 10: 118–132. doi:10.1175/1520-0450(1971)010<0118:AATFOC>2.0.CO;2.

Lewis, J. P. 1995. "Fast Normalized Cross-Correlation." *Vision Interface* 10 (1): 120–123.

Morimoto, A., T. Yanagi, and A. Kaneko. 2000. "Eddy Field in the Japan Sea Derived from Satellite Altimetric Data." *Journal of Oceanography* 56: 449–462. doi:10.1023/A:1011184523983.

Ninnis, R. M., W. J. Emery, and M. J. Collins. 1986. "Automated Extraction of Pack Ice Motion from Advanced Very High Resolution Radiometer Imagery." *Journal of Geophysical Research* 91: 10725–10734. doi:10.1029/JC091iC09p10725.

Park, K.-A., P. Cornillon, and D. L. Codiga. 2006. "Modification of Surface Winds near Ocean Fronts: Effects of Gulf Stream Rings on Scatterometer (Quikscat, NSCAT) Wind Observations." *Journal of Geophysical Research* 111: C03021. doi:10.1029/2005JC003016.

Park, K.-A., D. S. Ullman, K. Kim, J. Y. Chung, and K.-R. Kim. 2007. "Spatial and Temporal Variability of Satellite-Observed Subpolar Front in the East/Japan Sea." *Deep Sea Research Part I: Oceanographic Research Papers* 54: 453–470. doi:10.1016/j.dsr.2006.12.010.

Park, K.-A., H.-J. Woo, and J.-H. Ryu. 2012. "Spatial Scales of Mesoscale Eddies from GOCI Chlorophyll-*A* Concentration Images in the East/Japan Sea." *Ocean Science Journal* 47 (3): 347–358. doi:10.1007/s12601-012-0033-3.

Siegel, D. A., P. Peterson, D. J. McGillicuddy, S. Maritorena, and N. B. Nelson. 2011. "Bio-Optical Footprints Created by Mesoscale Eddies in the Sargasso Sea." *Geophysical Research Letters* 38 (13): L13608. doi:10.1029/2011gl047660.

Yang, H., J.-K. Choi, Y.-J. Park, H.-J. Han, and J.-H. Ryu. 2014. "Application of the Geostationary Ocean Color Imager (GOCI) to Estimates of Ocean Surface Currents." *Journal of Geophysical Research: Oceans* 119: 3988–4000. doi:10.1002/2014JC009981.

Yoder, J., L. Atkinson, S. Bishop, E. Hofmann, and T. Lee. 1983. "Effect of Upwelling on Phytoplankton Productivity of the Outer Southeastern United States Continental Shelf." *Continental Shelf Research* 1: 385–404. doi:10.1016/0278-4343(83)90004-3.